ARTICLE   OPEN

Future exacerbation of hot and dry summer monsoon extremes in India

Vimal Mishra [1,2 ✉], Kaustubh Thirumalai [3], Deepti Singh[4] and Saran Aadhar [1]

Summer monsoon (June-September) precipitation is crucial for agricultural activities in India. Extremes during the monsoon season can have deleterious effects on water availability and agriculture in the region. Here, we show that hot and dry extremes during the summer monsoon season significantly impact food production in India and find that they tend to occur during El Niño years during the observed record of 1951–2018. We then use an ensemble of climate simulations for the historic (1971–2000) and future (2006–2100) that capture this coupling between El Niño and the Indian monsoon to show that the frequency of concurrent hot and dry extremes increases by a factor of 1.5 under continued greenhouse warming during the 21st century. Despite projections of summer monsoon intensification on the order of ~10%, the rise in surface air temperatures as well as increase in rainfall variability contributes to more severe hot and dry monsoon extremes over India, thereby posing a substantial challenge to future food security in India.

INTRODUCTION

Food security in the Indian subcontinent is inextricably linked to summer monsoon rainfall. It is well-known that Indian monsoon variability significantly impacts food production and, therefore, affects the socioeconomic well-being of more than a billion people[1]. Several studies have documented the relationship between agriculture and excesses and deficits in monsoon rains across various regions of India[1–9]. Despite overall increasing rates of food production since the mid-20th century, mainly tied to technological advances and increased inputs during the Green Revolution, fluctuations in summer monsoon rainfall yet cause sharp anomalies in the yields of many staple crops. Given such a tight coupling between climate and agricultural production in a region with a rising population and nutritional demands, there is a pressing need to anticipate future changes in monsoon variability under greenhouse warming.

In particular, monsoon rainfall extremes can cause substantial crop damage across the subcontinent. Thus, considerable efforts have been devoted to the detection and attribution of extreme rainfall events over the observational period, and in simulations of future climate change[10–15]. However, due to the large uncertainty in model sensitivity and choice of metrics, debate persists regarding future changes in rainfall extremes, despite the consensus that the Indian monsoon will intensify in a warmer world[12].

Nevertheless, considerably less attention has been given to the combined impact of rainfall and air temperature extremes during the summer monsoon season over India. Concurrent hot and dry extremes are known to have a pronounced influence on food production, water availability, and human discomfort across the world[16–18]. In this work, we demonstrate the negative effect of seasonal hot and dry extremes on staple crop yields in India during the monsoon season. Next, we diagnose the potential drivers of these extremes using observations and link them to the El Niño Southern Oscillation (ENSO) phenomenon. Finally, we use

an ensemble of global warming simulations to investigate projections of the frequency of concurrent hot and dry extremes over India in the 21st century.

RESULTS

Concurrent hot and dry extremes and food production in India

The total food production of staple crops in India has nearly tripled over 1951–2016 (Fig. 1a) despite declining rainfall and increasing temperatures during the monsoon season (Supplementary Fig. 1). For instance, yields of food grain (cereals and pulses), rice, wheat, and cereals (Rice, Jowar, Bajra, Maize, Wheat, and Barley) have increased at a rate of 25, 27, 43, and 15.5 kg/ha, respectively, over this period. The significant rise in crop yields is attributable to refined agricultural management associated with the expansion of irrigation, fertilizers, and improved seeds after the green revolution[19]. However, year-to-year rainfall and temperature anomalies during the monsoon season (hereafter defined from June to September; JJAS) still have sizeable impacts on staple crop yields in India[20,21].

To address these anomalies in food production under the backdrop of an overall increasing trend, we apply a first-difference filter[22] to compilations of yearly crop yields (Fig. 1b). We find that the first difference of JJAS precipitation is significantly correlated (p-value < 0.05) to total food grain (r = 0.71) and rice (r = 0.70) yields in India, with decreased monsoon rainfall associated with reduced production. Furthermore, monsoon rainfall is positively correlated with wheat (r = 0.45) and cereal (r = 0.50) yields, indicating a significant yet indirect effect on crops grown outside the monsoon season. This indirect effect is primarily due to soil moisture storage during the monsoon season, which provides favorable conditions for agricultural growth in the post-monsoon season. Similarly, albeit with slightly weaker correlations, all-India averaged air temperature anomalies during the monsoon season are also associated with anomalies in crop yields (refer to Fig. 1b

[1]Civil Engineering, Indian Institute of Technology (IIT) Gandhinagar, Gandhinagar, Gujarat 382355, India. [2]Earth Sciences, Indian Institute of Technology (IIT) Gandhinagar, Gandhinagar, Gujarat 382355, India. [3]Department of Geosciences, University of Arizona, 1040 E. 4th Street, Tucson, AZ 85721, USA. [4]School of Environment, Washington State University, Vancouver, WA 98686, USA. ✉email: vmishra@iitgn.ac.in
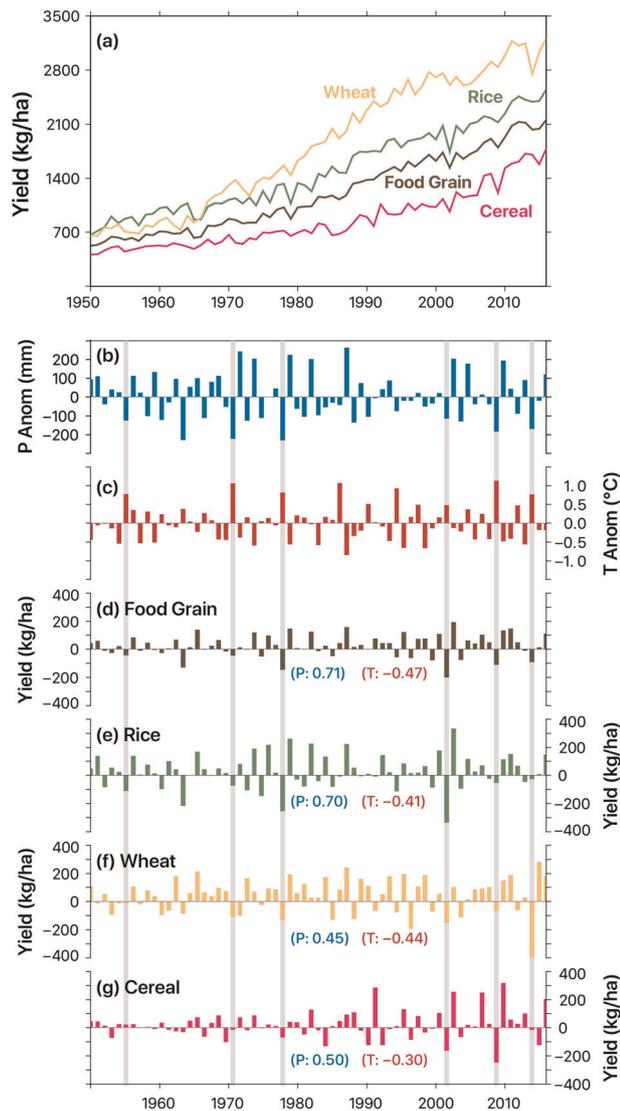
Fig. 1 Changes in food production and associated links with monsoon precipitation and temperature over India. a Changes in yield (kg/ha) of wheat, rice, food grain, and cereal in India from 1951–2016, **b** first difference of precipitation (mm) during the monsoon season (June to September) for 1951–2016, **c** same as (**b**) but for the June-to-September air temperature (°C), **d**–**g** first difference of food grain, rice, wheat, and cereal yield (kg/ha) during 1951–2016. The first difference was estimated by subtracting the value of the previous year from the current year. Vertical lines indicate precipitation anomalies with a deficit of more than 100 mm and temperature anomalies of more than 0.5 °C during the monsoon season. Such events occurred in 1957, 1972, 1979, 2002, 2009, and 2014, and were associated with significant reductions in food yield. Values in parenthesis indicate the correlation between food yield versus precipitation (*P*) and temperature (*T*). Precipitation and temperature anomalies are estimated using all-India averaged precipitation and temperature. Correlations between crop yield and precipitation/temperature were estimated for the entire period of 1951–2016.

for correlations). We find significant (*p*-value < 0.05) negative correlations between monsoon season air temperature and crop yields, with warmer temperatures linked to reduced production (Fig. 1). Moreover, the monsoon season rainfall explains more than 50% of the total variance in food grain and rice yields (Supplementary Table 1). On the other hand, the monsoon season temperature explains about 22% of the total variance of food

grain yields. The relative contribution of the monsoon season rainfall and temperature was estimated considering them together (Supplementary Table 2). The monsoon season rainfall has more than 40% contribution in food grain and rice yields.

Combining these inferences, we find that concurrent hot and dry monsoon seasons are associated with substantially reduced crop yields in India (Fig. 1). The top six years with deficits in monsoon rainfall larger than 100 mm and with concurrent temperature anomalies larger than 0.5 °C occurred in 1957 (precipitation deficit = −125 mm and temperature anomaly = 0.7 °C), 1972 (−223.8 mm, 1.0 °C), 1979 (−231 mm, 0.8 °C), 2002 (−115 mm, 0.5 °C), 2009 (−183 mm, 1.1 °C), and 2014 (−170 mm, 0.7 °C). These years are also associated with the largest anomalies in crop yields, with total food grain yield reduced by 41 (1957), 44 (1972), 146 (1979), 200 (2002), 111 (2009), and 92 (2014) kg/ha, respectively, (Fig. 1). The year 2002 is not as dry and hot as compared with the years 2009 and 2014. However, crop yields were considerably low for the year 2002 in comparison to years 2009 and 2014. The year 2002 was the worst monsoon season drought with a much larger areal extent (~54%) than in 2009 (~45%) and 2014 (~35%) (Supplementary Fig. 2). The year 1965 had crop yields lower than in 1972 and 1951. The 1965 drought was mainly centered in one of the most productive regions (i.e., Gangetic plain) in India (Supplementary Fig. 2). Since the all-India averaged crop yields were used in our analysis, location, areal extent, and timing of droughts (e.g., 1965 and 2002) might have affected the crop yields more than the noticeable concurrent hot and dry events. Overall, extreme dry and hot events are associated with significant reductions in rice, wheat, and cereal yields over this period as well (Fig. 1), thereby demonstrating the strong propensity of hot and dry extremes to induce anomalies in Indian food production.

Observed hot and dry extremes in India

What causes hot and dry monsoon extremes in India? We characterized these events using the standardized precipitation evapotranspiration index (SPEI[23]) and air temperature anomalies for the monsoon season. SPEI considers available water as the difference of precipitation and potential evapotranspiration (PET, see Methods for details). Monsoon seasons with SPEI less than −1 and temperature anomalies greater than 1 were categorized as concurrent hot and dry extremes. Although there are slight discrepancies compared with the events categorized using the first difference of monsoon rainfall and temperature (Fig. 1), SPEI provides a more robust assessment of dryness in the Indian monsoon region (see Methods for more details). Overall, India experienced seven (1951, 1972, 1979, 1987, 2009, 2014, and 2015) concurrent hot and dry monsoon seasons over the observed period of 1951–2018 (Fig. 2a, b and Supplementary Table 3). Out of these seven extreme seasons, four occurred after 1980 while three (2009, 2014, and 2015) occurred in the most recent decade (2009–2018) indicating an increased frequency of such events in recent time.

All the seven concurrent hot and dry monsoon extremes occurred during El Niño events, the positive phase of ENSO (Supplementary Fig. 3). We find that sea-surface temperature (SST) in the Niño3.4 region, central Pacific, an indicator of ENSO variability, are significantly correlated (*r* = 0.6; *p* < 0.05) with monsoon-season SPEI values over 1951–2018. Similarly, we also observe a significant relationship between monsoon season temperature anomalies and Niño3.4 SSTs (*r* = 0.43; *p* < 0.05). Out of the seven hot and dry monsoons during this period, three (1972, 1987, and 2015) were linked to strong El Niño events with Niño3.4 SST anomalies larger than 1.0 °C (Supplementary Fig. 3).

Although each extreme event is consistently associated with warm SSTs in the Pacific, the spatial pattern of these events over India is variable. However, each event induces intense warming
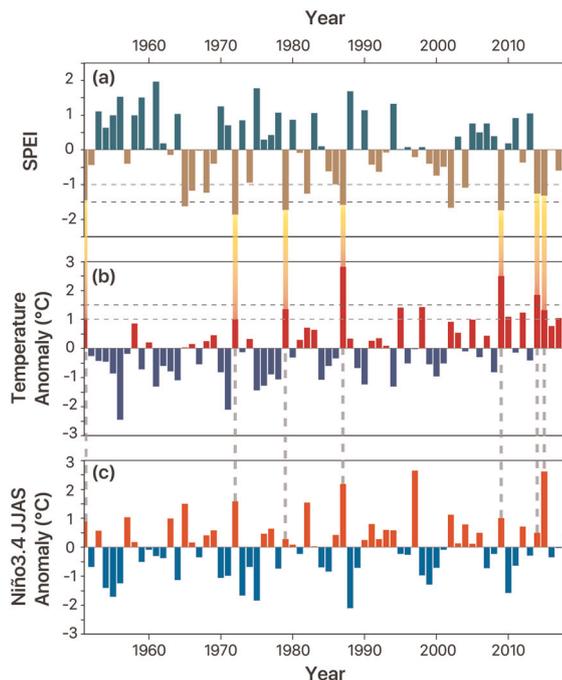
Fig. 2 Hot and dry extremes over India during the monsoon season (June-September) and associated links with El Niño over 1951–2018. a Four-month (June to September) Standardized Precipitation Evapotranspiration Index (SPEI) at the end of September from 1951 to 2018, **b** standardized temperature (*T*) anomaly during the monsoon season in India, **c** Niño 3.4 SST anomaly for the monsoon season during the same period. Gray vertical bars denote hot and dry monsoon anomalies with SPEI and T anomalies less than −1 and more than 1, respectively. 1987 and 2009 were identified as extreme hot and dry monsoon years with SPEI less than −1.5 while *T* anomaly more than 1.5 during the period of 1951–2018.

and drying across large swaths of India. For example, a large part of western and central India was affected by extreme dryness and heat in 1987, when SST patterns in the Pacific Ocean were characterized by El Niño conditions (Supplementary Fig. 3). Similarly, extreme hot and dry conditions affected a large part of northern and central India during the monsoon season of 2009 (Supplementary Fig. 3). The other five hot and dry extreme years (1951, 1972, 1979, 2014, and 2015) were also linked with warm SST anomalies over the central Pacific Ocean and similarly affected large parts of northern India (Supplementary Fig. 3).

To further explore the dynamics behind the observed SPEI values and Pacific SSTs during the monsoon season, we performed maximum covariance analysis (MCA, see Methods for more details) over the 1951–2018 period (Fig. 3a). The first leading mode exhibits an ENSO-like pattern that confirms a strong correlation between SPEI and SSTs over the central Pacific ($r = 0.6$; Fig. 3a, b). The second leading mode obtained from MCA has characteristics that somewhat resemble the Indian Ocean Dipole (IOD) pattern, and primarily affects rainfall in Southern India during the monsoon season (Supplementary Fig. 4c, d). Finally, the third leading mode from MCA points towards the role of Indian Ocean SSTs on monsoon-season rainfall over northern and southern India[24,25], where Indian ocean warming is associated with drying over the Gangetic Plain (Supplementary Fig. 4e, f). Thus, the dynamics of hot and dry extremes are tied to El Niño as well as Indian Ocean warming. However, the linkage of hot and dry extremes with ENSO may change under the global warming climate due to change in the Walker circulation[26–29]. Recent studies reported the weakening of the Walker circulation in observed climate due to rapid warming over the Indian Ocean in comparison to the Pacific Ocean[28,29].

Future monsoon extremes

How will hot and dry monsoon extremes change in the future? To address this question, we used simulations of the historic and

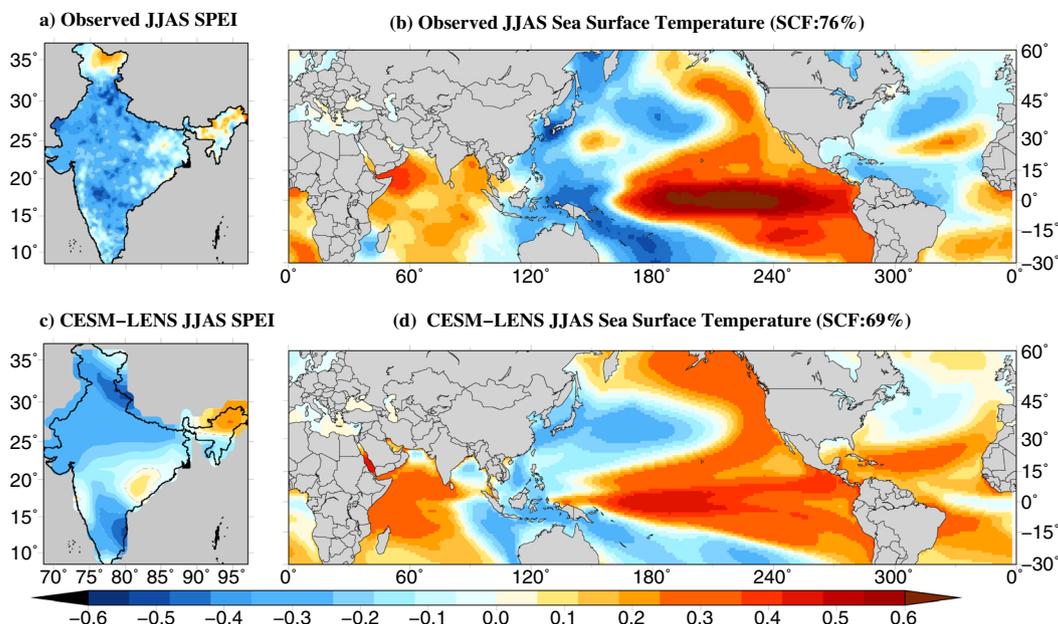**Fig. 3 Heterogeneous correlations between 4-month SPEI and SST anomalies for the monsoon season obtained using Maximum Covariance Analysis (MCA). a, b** Correlations for the observed SPEI and SST for the monsoon season obtained from the first leading mode of MCA for 1951–2018, and **c, d** composite of heterogeneous correlations between monsoon season SPEI and SST from the first leading mode of MCA from all 40 ensemble members of CESM-LENS. Numbers in brackets denote the squared covariance fraction (SCF) explained by the first leading mode. For CESM-LENS, we calculated the mean SCF from all ensemble members.
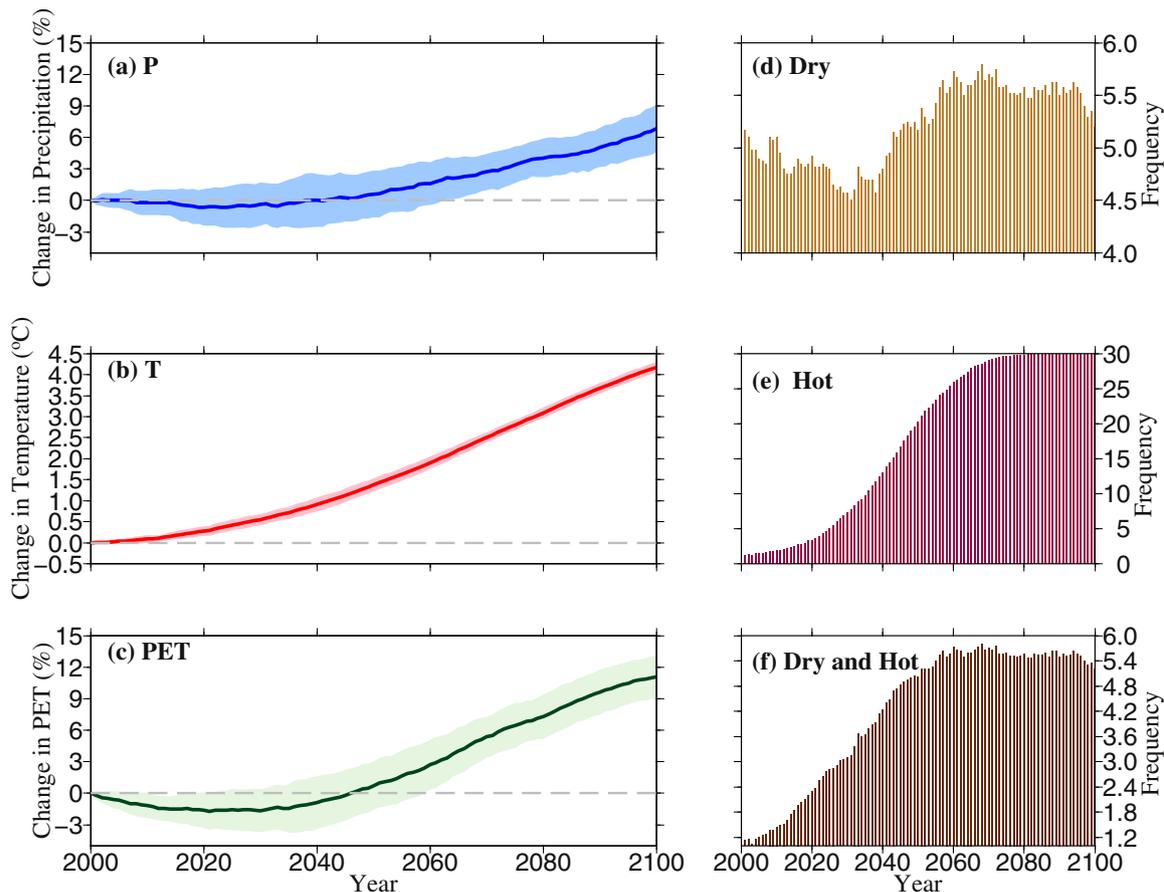
Fig. 4   Climate warming and future changes in hot and dry extremes over India. a Ensemble-mean 30-year average change in monsoon season precipitation (%) against the reference of 1971–2000 over 2000–2100 period based on 40 large ensemble LENS members, **b** same as in (**a**) but for the monsoon season temperature (*T*), **c** same as in (**a**) but for the monsoon season potential evapotranspiration (PET, %), **d** 30-year moving-mean frequency of extreme dry (SPEI ≤ −1) events, **e** 30-year moving-mean frequency of extreme hot (temperature anomaly ≥ 1.0), and **f** 30-year moving-mean frequency of extreme hot and dry events during 2000–2100 periods. Estimates in (**d**–**f**) are based on the ensemble mean of 40 LENS members.

future climate from the Community Earth System Model Version 1 Large Ensemble (CESM-LENS) for the high-emission scenario (RCP 8.5). This model realistically simulates the coupling between Indian monsoon rainfall and ENSO over the observed period (1951–2005) and is skilled at reproducing monsoon spatial patterns as well as seasonality (Supplementary Fig. 5a, c). Moreover, CESM-LENS is known to reproduce observed ENSO variability as well as ENSO-induced circulation and SST anomalies[18,30,31]. Our MCA exercise based on composites of correlations obtained in the first leading mode from all the ensemble members shows that CESM-LENS simulations capture ENSO-monsoon coupling over India reasonably well (Fig. 3c, d). In addition, the squared covariance explained by the first leading mode in the observations and LENS simulations is about 70%. The realism of CESM-LENS, consisting of model output from 40 ensemble member simulations of 20th and 21st-century climate[32], allows us to explore changes in future monsoon extremes over India.

In agreement with many other model simulations[12,33], the CESM-LENS also indicates that India is projected to witness increased monsoon rainfall (~6% increase by 2100) under future greenhouse warming (Fig. 4a). However, air temperature over India is also projected to increase by 4 °C on average by the end of the 21st century. This coupling results in a ~10% increase in potential evapotranspiration (PET), or atmospheric water demands (Fig. 4b, c). The increase in atmospheric water demands under a warmer climate with the effect of increased global mean CO_2 concentration (Supplementary Fig. 6) can reduce overall water

availability (i.e., the difference between precipitation and PET). Accordingly, the frequency of extreme dry (SPEI ≤ −1) monsoon seasons are projected to increase over the coming century (Fig. 4d), especially after the 2030s. Furthermore, alarmingly, extreme hot monsoon seasons, defined by today's standards, are likely to become normal after the 2040s (Fig. 4e), with CESM-LENS indicating that even more severe hot extremes will become regular toward the end of the 21st century. Finally, the combined influence of higher temperatures, variable monsoon rainfall, and rising PET results in an increased frequency of hot and dry monsoon extremes (Fig. 4f). As another metric of the impact of dryness and heat during the monsoon season, we estimated changes in surface soil moisture (10 cm) according to CESM-LENS (Supplementary Fig. 7). Soil moisture is a plant-centric measure of the atmospheric water demand[34]. We did not consider deeper soil moisture in our analysis to avoid the influence of high soil moisture persistence[35] on monsoon-season dry and hot extremes. This exercise reinforced our results with estimated changes in PET, wherein surface soil moisture is projected to decrease and the combination with increased warming results in the increased frequency of concurrent hot and dry extremes over the 21st century (Supplementary Fig. 8).

According to CESM-LENS, the main driver of hot and dry monsoon extremes over India is El Niño. As in the observations, the leading mode obtained from MCA on output from the CESM-LENS members indicates a strong correlation with El Niño (Fig. 3c, d). Although there are differences between the patterns in the

leading MCA mode from the simulations and the observations, the similarities are striking, with negative correlations across much of India and relatively weaker or positive correlations over eastern India. The second and third leading modes also resemble those in the observations, additionally testifying to the realism of the simulations and potentially suggesting that the dynamical controls on the monsoon remain intact over the coming century (Supplementary Figs 9, 10).

CESM-LENS simulations indicate future exacerbation of monsoon extremes in the latter half of the 21st century. The changes in all-India averaged air temperature and SPEI from all the ensemble members of CESM-LENS were evaluated during the monsoon season by dividing our dataset into two periods (1971–2000 and 2071–2100). Forcing changes dramatically at the end of the 21st century (Fig. 5). Similarly, two periods (1971–2000 and 2071–2100)

were used to evaluate the linkage between ENSO and concurrent hot and dry extremes during the summer monsoon (Fig. 6). A significant warming trend is projected during the monsoon season over India as shown by the kernel-density function of air temperature (Fig. 5a). Both the mean (Ranksum test) and variance (Kolmogorov–Smirnov (KS) test) of monsoon season air temperature are significantly (p-value < 0.05) different for 2071–2100 compared with the 1971–2000 period. Despite the substantial rise in air temperature, the normalized density for SPEI over the 2071–2100 period is not considerably different (though significant) due to the projected increase in rainfall (Fig. 5b).

We identify a total of 42 concurrent hot and dry monsoon years with SPEI less than −1 and air temperature anomaly greater than 1 °C in all the 40 ensemble members of CESM-LENS during 1971–2000 (30-years duration). The SST composite across these 42 extreme years
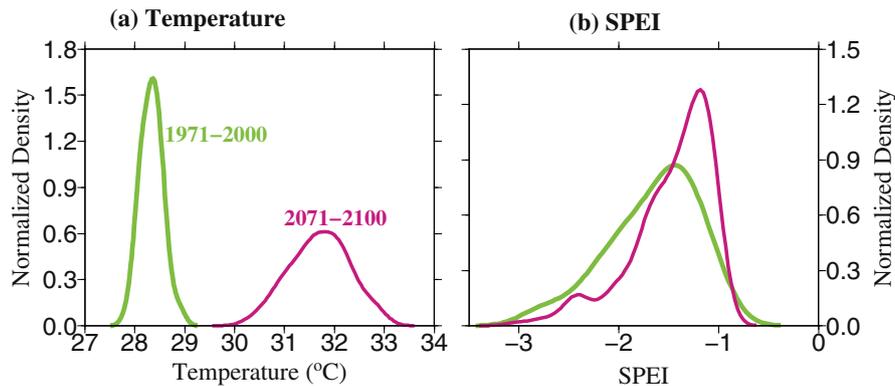

Fig. 5 Changes in the future likelihood of hot and dry monsoon extremes over India. Normalized densities of air temperature (left) and SPEI (right) across 40 LENS ensemble members for the period 1971–2000 (green) and 2071–2100 (pink) using kernel-density estimates. The changes in air temperature over these periods are significantly different both in mean (two-sided Ranksum test; p-value < 0.001) and variance (two-sided KS test; p-value < 0.001) whereas the change in SPEI is also significant (both p-values < 0.01).
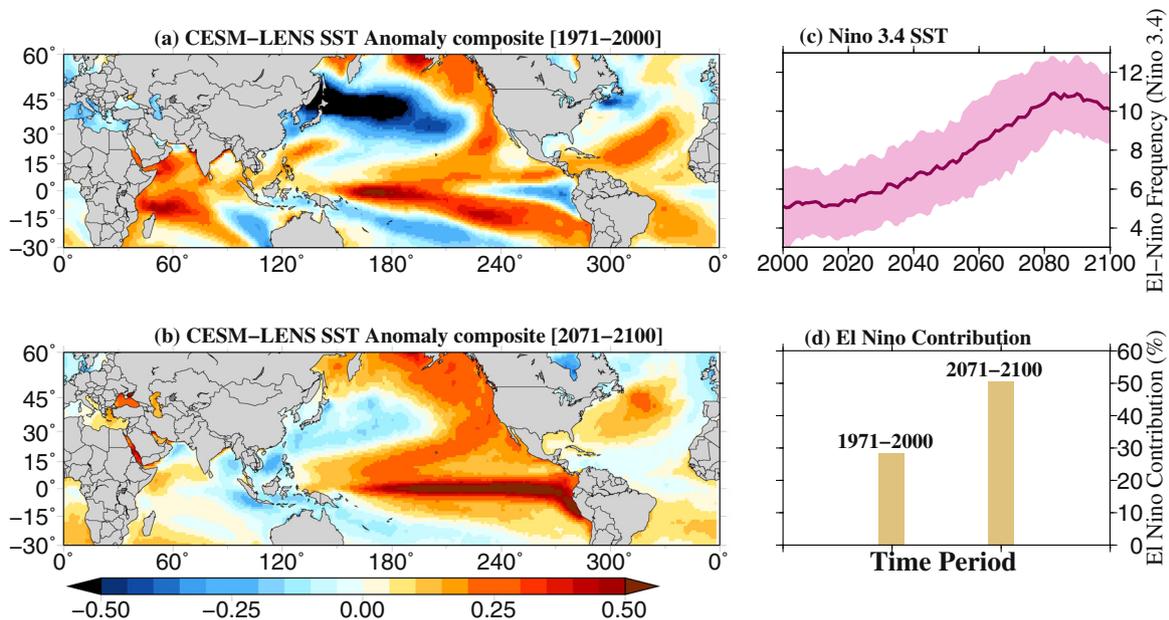

Fig. 6 El Niño and monsoon extremes in CESM-LENS. a, b Composite SST anomalies for hot and dry monsoon seasons during 1971–2000 and 2071–2100 from all ensemble members of CESM-LENS. The criteria for our choice of hot and dry extremes is a JJAS temperature anomaly greater than 1 °C and SPEI with values less than −1. **c** Change in the frequency of El-Nino (for the Niño 3.4 region; values greater than 0.5 °C) estimated from the ensemble mean of CESM-LENS using a 30-year moving-mean starting from 1971 with shaded regions indicating inter-member variability across all ensemble members. **d** Fraction of hot and dry monsoon extremes over India associated with El Niño (Niño3.4) during 1971–2000 and 2071–2100.
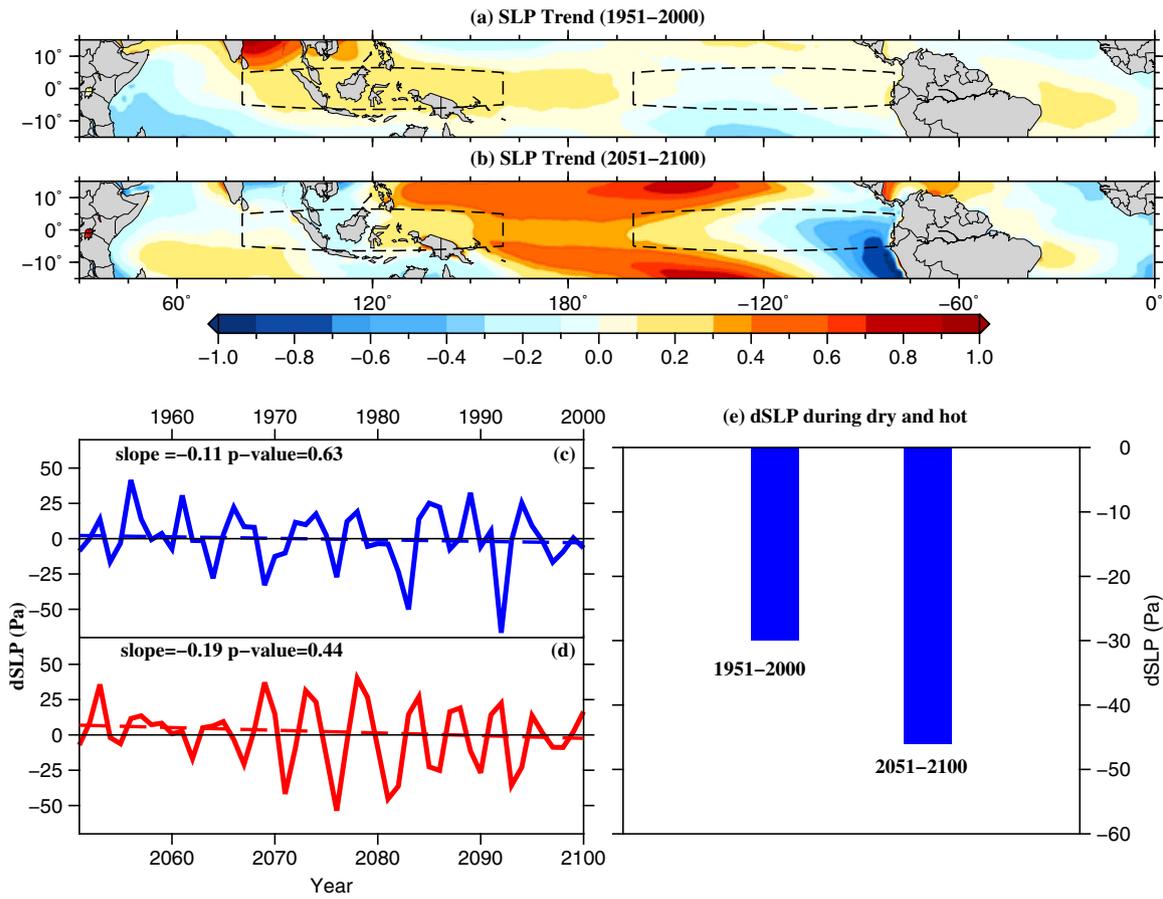
Fig. 7 Ensemble mean of linear trend in sea level pressure (SLP) from 40 ensemble estimated using CESM-LENS simulations during the historical (1951–2000) and the future climate (2051–2100). a, b Ensemble-mean linear trend in SLP during the monsoon season for the 1951–2000 and 2051–2100 periods. Mean trend over the domain 15°S–15°N, 0°–360° was removed from each grid to exclude the influence of global warming. Boxes (in **a, b**) indicate the regions used to define the large-scale Indo-Pacific SLP gradient index (dSLP). **c, d** Ensemble-mean dSLP (Pa) during 1951–2000 and 2051–2100 from all the ensemble members of CESM-LENS. **e** Composite of SLP gradient index (dSLP) during dry and hot extremes for the historical (1951–2000) and future (2051–2100) climate from all the ensemble members of CESM-LENS.

clearly indicates the influence of El Niño on hot and dry extremes (Fig. 6a). Similarly, based on 208 hot and dry monsoon seasons in the future period (2071–2100; 30-years duration in 40 ensemble members of CESM-LENS), these extremes are more strongly linked with El Niño (Fig. 6b). Given that the frequency of El Niño is projected to rise under future climate change[36,37], the fraction of extreme hot and dry monsoon years that occurred during El Niño years over the two periods (Fig. 6c, d). The association of El Niño (based on Niño3.4 SSTs) to concurrent hot and dry extremes is likely to rise by 20% over 2071–2100 compared with 1971–2000 (Fig. 6d). Across all the CESM-LENS ensemble members about 30% of the total hot and dry extremes occur with El Niño during 1971–2000 whereas that fraction increases to 50% over 2071–2100 (Fig. 6d). We note that our analysis does not investigate SST in the other ENSO regions[9], which could increase the contribution of El Niño to India's hot and dry monsoon extremes (Fig. 6d).

We evaluated the co-variability of atmosphere and ocean to identify the drivers of hot and dry extremes during the monsoon over India. The Walker circulation is known to play a key role during the positive phase of ENSO[26–29]. The trends in SLP and SLP gradient (between central and (western Pacific/Indian Ocean) in all the ensemble members of CESM-LENS (Fig. 7) were estimated to understand the strength of the Walker circulation[28]. To estimate the robust trend in the CESM-LENS ensemble members, slightly longer periods (1951–2000 and 2051–2100) in the historical and future climate were selected. SLP has increased over the Indian

Ocean/western Pacific (80°E–160°E, 5°N–5°S) while declined over the central/east Pacific Ocean (160°W–80°W, 5°N–5°S) in the historical (1951–2000) and projected to decline in the future (2051–2100). The increase in SLP over the western Pacific and the decline in the central Pacific show the weakening of the Walker circulation (Fig. 7). Moreover, the SLP gradient index (dSLP), which is the difference in SLP between the central Pacific (160°W–80°W, 5°N–5°S) and western Pacific (80°E–160°E, 5°N–5°S) oceans, represents the intensity of Walker circulation. SLP gradient is projected to decline more rapidly in the future (2051–2100) in comparison to the historical period of 1951–2000 (Fig. 7c, d). The composite analysis of SLP for all the hot and dry extremes shows that a weakening in the Walker circulation in the historical period, which is projected to continue in the future (Fig. 8a, b) and consistent with the previous study[38]. Similarly, the composite of SLP for hot and dry extremes that occurred during El-Nino shows even a stronger weakening of the Walker circulation, indicating the strong El-Nino teleconnection with Indian summer monsoon. Since the western Pacific and Indian Ocean SST is warming with a faster rate[24,28], the weakening in the Walker circulation may continue under the warming climate.

DISCUSSION
Addressing and anticipating future changes in climate extremes with continued greenhouse warming is of critical importance for regional

(a) SLP anomaly (Pa) composite during hot and dry extremes (1971–2000)

(b) SLP anomaly (Pa) composite during hot and dry extremes (2071–2100)

(c) SLP anomaly (Pa) composite during hot and dry extremes with ENSO (1971–2000)

(d) SLP anomaly (Pa) composite during hot and dry extremes with ENSO (2071–2100)
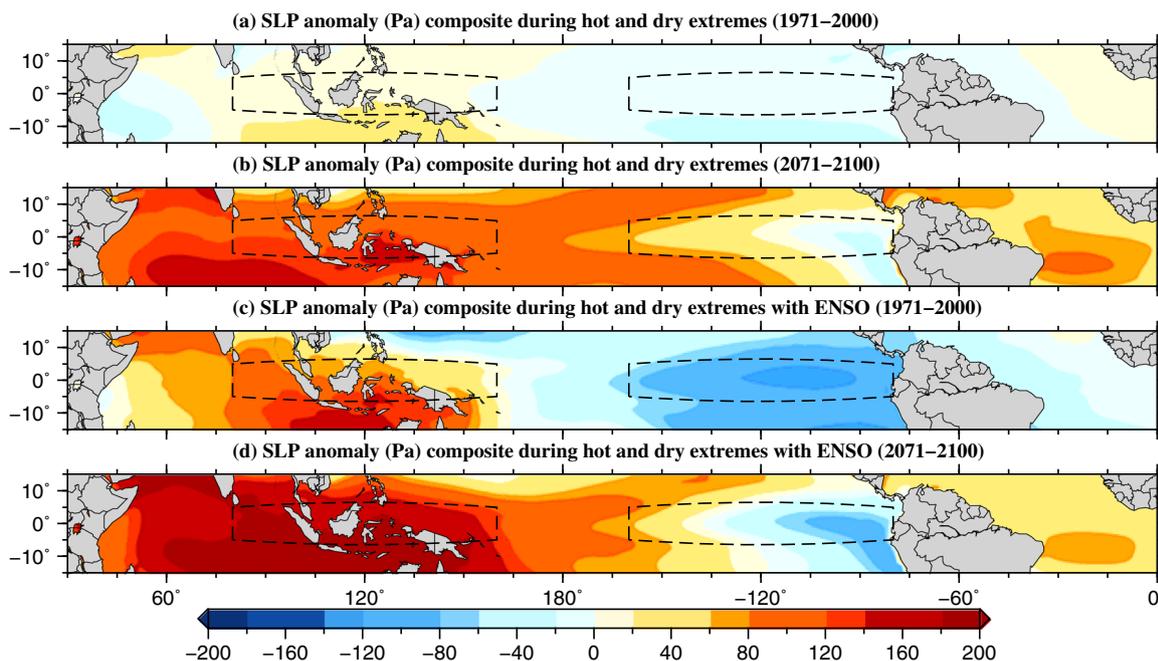
Fig. 8 Composites of sea level pressure (SLP) anomaly (Pa) during the hot and dry extremes and ENSO estimated using all the 40 members of CESM-LENS. a, b Composite of SLP anomaly (Pa) during the hot and dry extremes for historical (1971–2000) and future (2071–2100) from all ensemble members of CESM-LENS. **c, d** Composite of SLP anomaly (Pa) during hot and dry extremes that occurred during El-Nino for the historical (1971–2000) and future (2071–2100) from all ensemble members of CESM-LENS.

adaptation[39,40]. Thus far, due to an emphasis on rainfall extremes over the Indian subcontinent, changes in the magnitude and frequency of hot and dry monsoon years have largely been overlooked. In this work, we have shown how these events have already had considerable impacts on staple crop yields across India and long-term warming can increase the prevalence of hot and dry extremes. Moreover, we link the occurrence of these extremes over the Indian subcontinent to El Niño events in the Pacific Ocean. Despite a low number of El Niño events in the observational record, the CESM-LENS simulations facilitate conclusive statistics that long-term warming can worsen these ENSO-modulated events due to the weakening of the Walker circulation. Our analysis finds that concurrent hot and dry extremes will increase in frequency and magnitude over the coming century. According to CESM-LENS, in spite of seemingly stable SPEI projections due to moderate increases in future monsoon rainfall, the long-lived rise in surface-air temperatures will conspire with El Niño to yield extreme seasonal heat and dryness. Since our analysis is based on the single model (CESM-LENS), additional analyses with other global climate models that show reasonable skill in capturing the ENSO-monsoon relationship[41,42] can provide additional insights into the increasing contribution of El-Nino events in driving the rising concurrence of hot and dry extremes over India under the warming climate. Nonetheless, the increased severity of hot and dry monsoon extremes is likely to pose a substantial challenge to the future food security of the Indian subcontinent.

METHODS

Observed datasets

We obtained gridded (0.25 °C) precipitation and air temperature (1 °C) for 1951–2018 from India Meteorological Department (IMD). Air temperature data at 1 °C spatial resolution was regridded to 0.25 °C using bilinear interpolation to make it consistent with the precipitation dataset. Daily precipitation product from IMD has been developed using more than 6500 rain gauge stations located across India[43]. The gridded precipitation product captures the key features of the Indian summer monsoon precipitation. For instance, precipitation variability in the core monsoon season, western Ghats, and

north-eastern India are well captured. In addition, the gridded product resolves the influence of orography on precipitation reasonably well[44,45]. Daily temperature (at 1 °C) from IMD is developed using the station data from about 395 stations located in India. The temperature data showed warm bias in the northern regions of Himalaya due to sparse gage density, which has been reported in the previous studies[44,45]. We used yield (kg/ha) data for total food grain, rice, wheat, and cereals from the directorate of economics and statistics (https://eands.dacnet.nic.in/latest_20011.htm). All-India food grain and crop yields are available for the 1951–2016 period. We estimated the relationship between yields and precipitation and temperature during the monsoon season using the first difference[22] of time series. The first difference was estimated after removing the value of the previous year from the current year, which minimizes the influence of management practices (irrigation, fertilizer, and seed) on crop yields[22]. We estimated the relative importance[46] of the monsoon season rainfall and temperature in crop yield at 95% significant level.

CESM-LENS simulations

We used simulations from the Community Earth System Model Version 1 (CESM1) that consists of a large ensemble (CESM-LENS: hereafter) of 40 runs with the common period of 1920–2100[32]. The first ensemble of CESM (CESM-LENS01) covers the period of 1850–2100 and can be used to analyze the climate during the pre-industrial era. The 40 ensemble members of CESM-LENS are run using 40 different initial conditions, therefore, can be useful for understanding the role of internal climate variability on climate extremes. Moreover, a large number of runs from CESM-LENS enable us to conduct a more robust statistical analysis of climate extremes under the current and projected future climate[18]. We used surface temperature and precipitation from CESM-LENS simulations to estimate the changes in hot and dry extremes during the monsoon season.

Estimation of PET

We estimated atmospheric water demand (potential evapotranspiration: PET) to estimate standardized precipitation evapotranspiration index (SPEI[23]) considering 1971–2000 as the reference period. We estimated PET using Modified Penman–Monteith method for CESM-LENS datasets. Modified Penman–Monteith method considers the changes in surface resistance (resistance of vapor flow through stomata openings) with changes in atmospheric CO_2 concentration in the warming condition. Yang

et al.[47] incorporated the global mean atmospheric CO_2 concentration in the PET estimation:

$$PET = \frac{0.408\Delta(R_n - G) + \gamma\frac{900}{T+273}uD}{\Delta + \gamma[1 + u\{0.34 + 2.4 \times 10^{-4}([CO_2] - 300)\}]}$$

where R_n is net radiation at the surface, G is ground heat flux, Δ is the slope of the vapor pressure curve, u is wind speed, D is vapor pressure deficit, and γ is psychometric constant.

We obtained monthly global mean atmospheric CO_2 concentration from MPI-ESM-LR model for the historical (1920–2005) and RCP 8.5 (2006–2100) which is consistent with the atmospheric CO_2 concentration from CESM-LENS data (Supplementary Fig. 6). For observations (1951–2018), we used the Hargreaves–Samani[48] method to estimate the PET due to the lack of observed data required to estimate PET using the Modified Penman–Monteith method. We considered dry events with 4-month SPEI at the end of September, which represents cumulative available water (precipitation–PET) for the monsoon season, less than −1. Similarly, for hot monsoons, the temperature anomaly of more than 1 °C from the mean temperature for the reference period (1971–2000) was considered[49]. We considered the monsoon season affected by the hot and dry extremes if temperature anomaly was higher than 1 °C and SPEI was lower than −1, simultaneously. We estimated the mean frequency of hot, dry, and hot and dry monsoons from all the runs of CESM-LENS for each of the 30-years period starting from 1971.

Maximum covariance analysis (MCA)

We obtained NOAA extended reconstructed sea-surface temperature (SST, https://www.esrl.noaa.gov/psd/data/gridded/data.noaa.ersst.v5.html)[50] version 5 that is available at 2 °C spatial resolution and monthly temporal resolution to evaluate SST anomalies during hot and dry extremes in the observed period (1951–2018). Surface temperature (TS) from CESM-LENS was used to identify the SST anomalies during the historic and future periods. We obtained Niño 3.4 (5°N–5°S, 170°W–120°W) from National Center for Atmospheric Research (NCAR: https://climatedataguide.ucar.edu/climate-data/nino-sst-indices-nino-12-3-34-4-oni-and-tni) to evaluate the linkage between El Niño Southern Oscillation (ENSO) and hot and dry extremes in India. We estimated Niño 3.4 (5°N–5°S, 170°W–120°W) using the monsoon season SST. Notwithstanding ENSO peaks in boreal winter, we focused on the monsoon season as monsoon season SST in the Pacific Ocean is strongly associated with the summer monsoon precipitation over India[25,51,52]. Since the monsoon season SST has a strong trend under the future climate, to estimate SST anomalies for the selected Niño regions we removed secular trends[53] from SST time series using ensemble empirical mode decomposition (EEMD)[54]. In contrast to the common detrending methods, EEMD considers both linear and non-linear trends in data (Supplementary Fig. 10). We find a good agreement between Niño 3.4 based on Hadley Centre SST dataset (HadSST) and estimated using EEMD (Supplementary Figs 11, 12). SST anomalies were estimated for the monsoon season in the observed and CESM-LENS datasets after removing the trend using EEMD. We used maximum covariance analysis (MCA)[55] to evaluate the linkage between SST anomalies and hot and dry extremes over India. The MCA provides leading modes of coupled variability of SST and SPEI and heterogeneous correlation can be used to understand the strength of relationship in each leading mode[25].

Using the LENS-CESM sea level pressure (SLP) data, we estimated the SLP gradient index (dSLP) from the difference in SLP averaged over the central/east Pacific (160°W–80°W, 5°S–5°N) and over the Indian Ocean/west Pacific (80°E–160°E, 5°S–5°N)[28]. The SLP gradient, which represents the strength of the Walker circulation, was computed for the monsoon season. A positive SLP gradient means a strong Walker circulation while a negative gradient shows a weak Walker circulation, representative of El-Nino-like conditions. Moreover, SLP gradient was identified as a better proxy than wind for the Walker circulation[28]. Trends in the SLP were estimated using the non-parametric Mann–Kendall[56,57] and Sen's slope[58] methods. The influence of serial and spatial correlations in trend estimation was considered using modified method[59].

DATA AVAILABILITY

The data that support the findings of this study are available from the authors on reasonable request to the corresponding author.

REFERENCES

1. Gadgil, S. & Gadgil, S. The Indian monsoon, GDP and agriculture. *Econ. Polit. Wkly.* **41**, 4887–4895 (2006).
2. Parthasarathy, B., Rupa Kumar, K. & Munot, A. Forecast of rainy season foodgrain production based on monsoon rainfall. *Indian J. Agric. Sci.* **62**, 1–8 (1992).
3. Krishna Kumar, K., Rupa Kumar, K., Ashrit, R. G., Deshpande, N. R. & Hansen, J. W. Climate impacts on Indian agriculture. *Int. J. Climatol.* **24**, 1375–1393 (2004).
4. Milesi, C. et al. Decadal variations in NDVI and food production in India. *Remote Sens.* **2**, 758–776 (2010).
5. Prasanna, V. Impact of monsoon rainfall on the total foodgrain yield over India. *J. Earth Syst. Sci.* **123**, 1129–1145 (2014).
6. Davis, K. F., Chhatre, A., Rao, N. D., Singh, D. & Defries, R. Sensitivity of grain yields to historical climate variability in India. *Environ. Res. Lett.* **14**, 064013 (2019).
7. DeFries, R. et al. Synergies and trade-offs for sustainable agriculture: Nutritional yields and climate-resilience for cereal crops in Central India. *Glob. Food Security* **11**, 44–53 (2016).
8. Davis, K. F. et al. Assessing the sustainability of post-Green Revolution cereals in India. *Proc. Natl Acad. Sci. USA* https://doi.org/10.1073/pnas.1910935116 (2019).
9. Singh, D. et al. Climate and the Global Famine of 1876–78. *J. Clim.* **31**, 9445–9467 (2018).
10. Goswami, B. N., Venugopal, V., Sengupta, D., Madhusoodanan, M. S. & Xavier, P. K. Increasing trend of extreme rain events over india in a warming environment. *Science* **314**, 1442–1445 (2006).
11. Singh, D., Tsiang, M., Rajaratnam, B. & Di, N. S. Observed changes in extreme wet and dry spells during the South Asian summer monsoon season. *Nat. Clim. Chang.* **4**, 1–6 (2014).
12. Singh, D., Ghosh, S., Roxy, M. K. & McDermid, S. Indian summer monsoon: extreme events, historical changes, and role of anthropogenic forcings. *Wiley Interdiscip. Rev. Clim. Chang.* **10**, e571 (2019).
13. Ghosh, S., Das, D., Kao, S. C. & Ganguly, A. R. Lack of uniform trends but increasing spatial variability in observed Indian rainfall extremes. *Nat. Clim. Chang.* **2**, 86–91 (2012).
14. Roxy, M. K. et al. A threefold rise in widespread extreme rain events over central India. *Nat. Commun.* **8**, 1–11 (2017).
15. Mukherjee, S., Aadhar, S., Stone, D. & Mishra, V. Increase in extreme precipitation events under anthropogenic warming in India. *Weather Clim. Extrem.* https://doi.org/10.1016/J.WACE.2018.03.005 (2018).
16. Overpeck, J. T. Climate science: the challenge of hot drought. *Nature* **503**, 350–351 (2013).
17. Griffin, D. & Anchukaitis, K. J. How unusual is the 2012–2014 California drought? *Geophys. Res. Lett.* **41**, 9017–9023 (2014).
18. Thirumalai, K., DInezio, P. N., Okumura, Y. & Deser, C. Extreme temperatures in Southeast Asia caused by El Ninō and worsened by global warming. *Nat. Commun.* **8**, 1–8 (2017).
19. Siegfried, T. et al. Modeling irrigated area to increase water, energy, and food security in semiarid India. *Weather, Clim., Soc.* **2**, 255–270 (2010).
20. Mall, R. K., Singh, R., Gupta, A., Srinivasan, G. & Rathore, L. S. Impact of climate change on Indian agriculture: a review. *Climatic Change* **78**, 445–478 (2006).
21. Lobell, D. B., Sibley, A. & Ivan Ortiz-Monasterio, J. Extreme heat effects on wheat senescence in India. *Nat. Clim. Chang.* **2**, 186–189 (2012).
22. Lobell, D. B. & Field, C. B. Global scale climate-crop yield relationships and the impacts of recent warming. *Environ. Res. Lett.* **2**, 014002 (2007).
23. Vicente-Serrano, S. M., Beguería, S. & López-Moreno, J. I. A multiscalar drought index sensitive to global warming: The standardized precipitation evapo-transpiration index. *J. Clim.* **23**, 1696–1718 (2010).
24. Roxy, M. K. et al. Drying of Indian subcontinent by rapid Indian Ocean warming and a weakening land-sea thermal gradient. *Nat. Commun.* **6**, 7423 (2015).
25. Mishra, V., Smoliak, B. V., Lettenmaier, D. P. & Wallace, J. M. A prominent pattern of year-to-year variability in Indian Summer Monsoon Rainfall. *Proc. Natl Acad. Sci. USA* **109**, 7213–7217 (2012).
26. Bayr, T., Dommenget, D., Martin, T. & Power, S. B. The eastward shift of the Walker Circulation in response to global warming and its relationship to ENSO variability. *Clim. Dyn.* **43**, 2747–2763 (2014).
27. Power, S. B. & Smith, I. N. Weakening of the Walker Circulation and apparent dominance of El Niño both reach record levels, but has ENSO really changed? *Geophys. Res. Lett.* **34**, L18702 (2007).
28. Vecchi, G. A. et al. Weakening of tropical Pacific atmospheric circulation due to anthropogenic forcing. *Nature* **441**, 73–76 (2006).
29. Tokinaga, H., Xie, S. P., Deser, C., Kosaka, Y. & Okumura, Y. M. Slowdown of the Walker circulation driven by tropical Indo-Pacific warming. *Nature* **491**, 439–443 (2012).
30. DiNezio, P. N. et al. A 2 year forecast for a 60–80% chance of La Niña in 2017–2018. *Geophys. Res. Lett.* **44**, 11,624–11,635 (2017).

31. DiNezio, P. N., Deser, C., Okumura, Y. & Karspeck, A. Predictability of 2-year La Niña events in a coupled general circulation model. *Clim. Dyn.* **49**, 4237–4261 (2017).

32. Kay, J. E. et al. The Community Earth System Model (CESM) Large Ensemble Project: a community resource for studying climate change in the presence of internal climate variability. *Bull. Am. Meteorol. Soc.* **96**, 1333–1349 (2015).

33. Menon, A., Levermann, A., Schewe, J., Lehmann, J. & Frieler, K. Consistent increase in Indian monsoon rainfall and its variability across CMIP-5 models. *Earth Syst. Dyn.* **4**, 287–300 (2013).

34. Swann, A. L. S., Hoffman, F. M., Koven, C. D. & Randerson, J. T. Plant responses to increasing CO_2 reduce estimates of climate impacts on drought severity. *Proc. Natl Acad. Sci. USA* https://doi.org/10.1073/pnas.1604581113 (2016).

35. Mishra, V. et al. Reconstruction of droughts in India using multiple land surface models (1951-2015). *Hydrol. Earth Syst. Sci.* **2000**, 1–22 (2018).

36. Cai, W. et al. ENSO and greenhouse warming. *Nat. Clim. Change* **5**, 849–859 (2015).

37. Cai, W. et al. Increased variability of eastern Pacific El Niño under greenhouse warming. *Nature* **564**, 201–206 (2018).

38. Cai, W. et al. Increasing frequency of extreme El Niño events due to greenhouse warming. *Nat. Clim. Chang.* **4**, 111–116 (2014).

39. Fedoroff, N. V. et al. Radically rethinking agriculture for the 21st century. *Science* **327**, 833–834 (2010).

40. Anderson, W. B., Seager, R., Baethgen, W., Cane, M. & You, L. Synchronous crop failures and climate-forced production variability. *Sci. Adv.* **5**, eaaw1976 (2019).

41. Li, X. & Ting, M. Recent and future changes in the Asian monsoon-ENSO relationship: Natural or forced? *Geophys. Res. Lett.* **42**, 3502–3512 (2015).

42. Mishra, S. K., Sahany, S., Salunke, P., Kang, I.-S. & Jain, S. Fidelity of CMIP5 multi-model mean in assessing Indian monsoon simulations. *npj Clim. Atmos. Sci.* **1**, 1–8 (2018).

43. Pai, D. S. et al. Development of a new high spatial resolution (0.25° × 0.25°) Long Period (1901–2010) daily gridded rainfall data set over India and its comparison with existing data sets over the region. *Mausam* **65**, 1–18 (2014).

44. Shah, R. & Mishra, V. Evaluation of the reanalysis products for the monsoon season droughts in India. *J. Hydrometeorol.* **15**, 1575–1591 (2014).

45. Mahto, S. S. & Mishra, V. Does ERA-5 outperform other reanalysis products for hydrologic applications in India? *J. Geophys. Res. Atmos.* https://doi.org/10.1029/2019JD031155 (2019).

46. Silber, J. H., Rosenbaum, P. R. & Ross, R. N. Comparing the contributions of groups of predictors: Which outcomes vary with hospital rather than patient characteristics? *J. Am. Stat. Assoc.* **90**, 7–18 (1995).

47. Yang, Y., Roderick, M. L., Zhang, S., McVicar, T. R. & Donohue, R. J. Hydrologic implications of vegetation response to elevated CO_2 in climate projections. *Nat. Clim. Change* **9**, 44–48 (2019).

48. Hargreaves, G. H. & Samani, Z. A. Reference crop evapotranspiration from temperature. *Appl. Eng. Agric.* **1**, 96–99 (1985).

49. Diffenbaugh, N. S., Swain, D. L. & Touma, D. Anthropogenic warming has increased drought risk in California. *Proc. Natl Acad. Sci. USA* **112**, 3931–3936 (2015).

50. Huang, B. et al. Extended reconstructed sea surface temperature version 4 (ERSST. v4). Part I: Upgrades and intercomparisons. *J. Clim.* **28**, 911–930 (2015).

51. Mishra, V. Long-term (1870–2018) drought reconstruction in context of surface water security in India. *J. Hydrol.* **580**, 124228 (2020).

52. Zhou, Z., Xie, S. & Zhang, R. Variability and predictability of Indian rainfall during the monsoon onset month of June. *Geophys. Res. Lett.* **46**, 14782–14788 (2019).

53. Wu, Z., Huang, N. E., Wallace, J. M., Smoliak, B. V. & Chen, X. On the time-varying trend in global-mean surface temperature. *Clim. Dyn.* **37**, 759–773 (2011).

54. Wu, Z. & Huang, N. E. Ensemble empirical mode decomposition: a noise-assisted data analysis method. *Adv. Adapt. Data Anal.* **1**, 1–41 (2009).

55. Bretherton, C. S., Smith, C. & Wallace, J. M. An intercomparison of methods for finding coupled patterns in climate data. *J. Clim.* **5**, 541–560 (1992).

56. Kendall, M. G. *Rank Correlation Methods* (Charles Griffin, San Francisco, Calif., 1975).

57. Mann, H. B. Nonparametric tests against trend. *Econometrica* **13**, 245 (1945).

58. Sen, P. K. Estimates of the regression coefficient based on Kendall's tau. *Source J. Am. Stat. Assoc.* **63**, 1379–1389 (1968).

59. Yue, S. & Wang, C. Y. Applicability of prewhitening to eliminate the influence of serial correlation on the Mann-Kendall test. *Water Resour. Res.* **38**, 4-1–4-7 (2002).

AUTHOR CONTRIBUTIONS
V.M. conceived the idea and designed the study with inputs from K.T. and D.S. S.A. prepared the data from CESM-LENS ensemble. V.M. conducted the analysis. V.M. and S.A. worked on the dynamics using SST and SLP datasets. V.M. and K.T. wrote the initial draft. V.M., K.T., and D.S. improved the discussion and results.

COMPETING INTERESTS
The authors declare no competing interests.

ADDITIONAL INFORMATION
Supplementary information is available for this paper at https://doi.org/10.1038/s41612-020-0113-5.

Correspondence and requests for materials should be addressed to V.M.

Reprints and permission information is available at http://www.nature.com/reprints

Publisher's note Springer Nature remains neutral with regard to jurisdictional claims in published maps and institutional affiliations.